On the motions of the offset impact oscillator

1984 J. Phys. A: Math. Gen. 17 1791

(http://iopscience.iop.org/0305-4470/17/9/015)

J. Phys. A: Math. Gen. 17 (1984) 1791–1803. Printed in Great Britain

On the motions of the offset impact oscillator

M B Hindmarsh† and D J Jefferies‡
Clarendon Laboratory, Oxford OX1 3PU, UK

Received 12 August 1983, in final form 9 February 1984

Abstract. The motions of a periodically forced, damped, harmonic oscillator with one degree of freedom, impacting with no energy loss against a wall, are considered. In the 'offset' case considered here, the wall is not at the rest point of the oscillator. The regions of the stability of single impact orbits are calculated as functions of the forcing amplitude and frequency. A digital simulation is carried out, producing multi-impact orbits, flip and tangent bifurcations and chaotic attractors. Hysteresis between attractors is observed, and crises of the attractor are found which are not immediately identifiable with the collisions of unstable periodic and chaotic attractors. Some return maps for chaotic motions are plotted, providing evidence that the attractors do not have integer dimension; the families of curves do, however, show local structures which may be identified with nearby stable motions.

1. Introduction

Much interest has been aroused lately in the behaviour of nonlinear dissipative dynamical systems, and in particular in the use of two-dimensional mappings on the phase space of systems with one degree of freedom. (See Ott 1981 for a review.) The impact oscillator is computationally one of the simplest such systems one can think of; it consists of a one-dimensional damped simple harmonic oscillator which bounces elastically (i.e. without loss of energy) against a wall or stop. The mathematical definition is given in § 2. The equations of motion for this nonlinear system are particularly easy to compute, and as is shown below, it is possible to derive theoretical bounds for some of the possible orbits which makes the model of more than computational interest.

Figure 1 shows one visualisation of the system. The spring is driven sinusoidally and is stress free when the displacement is zero. The mass bounces on a perfectly elastic wall at position x_0 which may be greater or less than zero. The rest point of the oscillator is either at $x = x_0$ for $x_0 < 0$ or at $x = 0$ for $x_0 > 0$. In both cases there are trivial motions; if $x_0 > 0$ the mass may never hit the wall, and if $x_0 < 0$ the mass may never leave the wall. In both cases there are also periodic impacting motions for sufficient drive amplitude; each impact is characterised by the impact velocity (v) and the phase (ϕ) of the drive at the time of impact. In order to study the bifurcations of the system it suffices to study the behaviour of the values of the impact velocity v and

† Present address: Department of Theoretical Physics, Imperial College, London, UK.
‡ Present address: Department of Electronic and Electrical Engineering, University of Surrey, Guildford GU2 5XH, UK.

0305-4470/84/091791 + 14$02.25

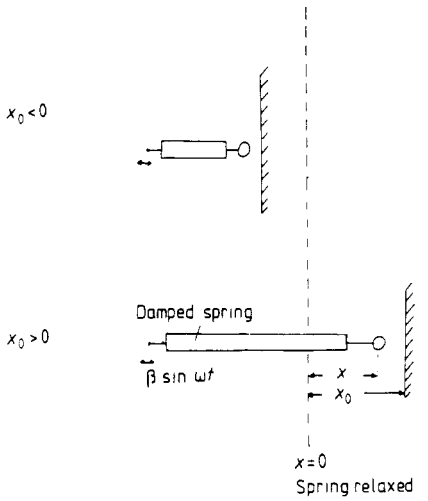

Figure 1. A visualisation of the offset impact oscillator.

phase ϕ of the drive at impact; between impacts the differential equation describing the motion is linear and has a unique solution for the initial conditions set by the impact. There are, therefore, no bifurcations of the system other than those revealed by a study of the impact values.

These impact values may be repeated at every mth impact ($m = 1, 2, 3, \ldots$) and during the interval between repeating impact values, n periods of the drive may have occurred ($n = 1, 2, 3, \ldots$). We refer to this situation as a periodic m-impact period-n orbit, where the orbit is the trajectory of the system in phase space.

The variables affecting the motion are the drive amplitude β, the drive angular frequency ω (the natural angular frequency of the unconstrained undamped system is scaled to unity), the damping coefficient α and the position of the wall at x_0. When the control parameters drive amplitude β or drive frequency ω are varied smoothly through the values at which bifurcation occurs, the trajectory changes smoothly even though there is a discontinuous change in the numbers n and m which describe the limiting periodic motions. The relaxation time for the trajectory to approach equilibrium increases as (β, ω) approach their bifurcation values from either side.

Shaw and Holmes (1982) (SH), who use a restitution coefficient r rather than damping, to make the map contracting, and Thompson and Ghaffari (1982) (TG) both set $x_0 = 0$, which results in the drive amplitude being unimportant. Both these studies report that as the drive frequency is changed, period doubling occurs from both harmonic ($n = 1$) and subharmonic ($n > 1$) solutions. Stable m-impact period-n orbits evolve into stable $2m$-impact period-$2n$ orbits as the drive frequency ω is slowly varied. These $(2m, 2n)$ periods in turn double repeatedly at successively smaller increments of ω until for values of ω above the 'accumulation point' chaotic motion occurs in which the impact values cease to be periodic and exhibit the familiar (Ott 1981) strange attracting behaviour. SH obtain expressions for bounds on the restitution coefficient r and the drive frequency ω for stable 1-impact orbits, and they establish that 'supercritical flip bifurcations' (Ott 1981) occur at the boundaries of the stable regions in the $r\omega$ plane.

In the offset case studied here, we find that flip bifurcation can also occur with changes in drive amplitude ($\beta/|x_0|$ when scaled to the wall position), and that tangent bifurcations (Ott 1981), whose general characteristic is that periodic motions appear

from chaos preceeded by intermittency, occur (Manneville and Pomeau 1979 and Pomeau and Manneville 1980). We have not found unequivocal evidence for this type of intermittency although it has been observed in a nonlinear transmission line constructed from eight coupled offset impact oscillators (Usher and Jefferies 1983), complete with laminar phases and aperiodic bursts.

There are tangent bifurcations predicted from the analysis of the stability of 1-impact orbits (see § 4) but there is also hysteresis when moving through the bifurcation—the tangent bifurcation only appears when approached from the stable orbit. Very often there is a coexisting stable orbit into which the system drops rather than exhibiting intermittency and chaos. Figure 3 shows this: the tangent bifurcation from a period-2 1-impact orbit occurs at the expected value ($\beta = 1.495$) when approached from above, and drops into a stable 1-impact orbit of period 1. If β is then increased again, this period-1 orbit undergoes flip bifurcations to chaos before settling into the original period-2 orbit.

The Poincaré maps themselves show clearly a Henon-like structure in the chaotic regions (Henon 1976). In addition, after nearly every sequence of period doubling bifurcations, crises occur, (Grebogi *et al* 1982) in which there are sudden changes in the bounds of the motion. The return map of the attractor is highly folded in the chaotic region and the attractor appears to have non-integer dimension, consisting of families of curves, regions of which are identifiable with stable periodic orbits that exist near the chaotic region. Robinson (1982) has made an experimental analogue electronic study of the piecewise linear system, and also reports period doubling, chaotic motion, and hysteresis, in the case of large slope ratio which approximates to the offset impact oscillator. Cascais *et al* (1983) and Jeffries and Perez (1982, 1983) and Perez and Jeffries (1982) have studied an RCL circuit with a varactor diode as a nonlinear capacitance, which shows similar behaviour, including the Henon-like Poincaré map and a folded (possibly non-integer-dimensional) return map of the attractor. (Iooss 1979).

2. The system

The impact oscillator is a limiting case as $\omega_1 \to \infty$ of the one-dimensional piecewise linear system

$$\ddot{x} + 2\alpha\dot{x} + H(x) = \beta \cos(\omega t) \qquad H(x) = \begin{cases} x & x < x_0 \\ x_0 - (1-\omega_1^2)x & x > x_0 \end{cases} \tag{1}$$

where α is the damping coefficient, β is the forcing amplitude and ω is the forcing frequency (we keep as closely as possibly to the notation of SH for convenience). In this limit,

$$\dot{x}(t) \to -\dot{x}(t) \qquad \text{when} \qquad x = x_0.$$

The motion is restricted to $x < x_0$. The general solution of the equation with initial conditions

$$x(t_0) = x_0 \qquad \dot{x}(t_0) = y_0$$

is, if $\alpha < 1$,

$$x(t; t_0, y_0) = \gamma \cos(\omega t) + \delta \sin(\omega t) + \{A \cos[\Omega(t-t_0)] + B \sin[\Omega(t-t_0)]\} \exp[-\alpha(t-t_0)] \tag{2}$$

where

$$\gamma = (1-\omega^2)\beta/\Delta \qquad \delta = 2\alpha\omega\beta/\Delta \qquad \Delta = (2\alpha\omega)^2 + (1-\omega^2)^2$$

$$\Omega = (1-\alpha^2) \qquad c_0 = \cos(\omega t_0) \qquad s_0 = \sin(\omega t_0) \qquad A = x_0 - \gamma c_0 - \delta s_0$$

$$B = [y_0 + \alpha x_0 + s_0(\gamma\omega - \delta\alpha) - c_0(\gamma\alpha + \delta\omega)]/\Omega$$

$$\dot{x}(t; t_0, y_0) = y(t; t_0, y_0) = \omega[\delta\cos(\omega t) - \gamma\sin(\omega t)] + \{(\Omega B - \alpha A)\cos[\Omega(t-t_0)] - (\Omega A + \alpha B)\sin[\Omega(t-t_0)]\}\exp[-\alpha(t-t_0)]. \tag{3}$$

If $x_0 = 0$ then β scales out completely. When $x_0 \neq 0$, only the relative size of β and x_0 are important, and β and x may be replaced by $\beta/|x_0|$ and $x/|x_0|$. Thus in the present case we may set $x_0 = \pm 1$ and vary β.

3. The Poincaré map and the Jacobian matrix

The equation of motion (1) maybe rewritten, between impacts, as two coupled first-order differential equations

$$\dot{x} = y \qquad \dot{y} = -2\alpha y - x + \beta\cos(\omega t).$$

The time evolution of the system from some set of initial conditions then can be identified with unique paths in (x, y) phase space. The Poincaré section may be conveniently taken to be $\{(x, y): x = x_0, y > 0\}$. The mapping of successive points $\boldsymbol{p}_k = (t_k, y_k)$ in the Poincaré section

$$\boldsymbol{p}_{k+1} = F(\boldsymbol{p}_k) \tag{4}$$

can not, in general be expressed in analytic form, since the time t_{k+1} is a root of a transcendental equation involving t_k, y_k. Nor is it continuous, for a small variation of $\boldsymbol{p}_k$ can lead to the expected impact being missed. However, the matrix (m) whose determinant is the Jacobian D where

$$D = \partial(t_{k+1}, y_{k+1})/\partial(t_k, y_k) \tag{5}$$

is calculable and SH have shown that for a 1-impact period-n orbit (that is, one which produces an impact with the same phase of the drive, $\omega t \bmod 2\pi$ and velocity every n forcing periods) with unity restitution coefficient and

$$y_{k+1} = y_k \qquad t_{k+1} = t_k + 2\pi n/\omega$$

its determinant (the Jacobian itself) and trace are given by

$$D = \det(m) = E^2 \tag{6}$$

$$T = \mathrm{Tr}(m) = 2E[(\beta c_k - x_0)s/\Omega y_k - c) \tag{7}$$

$$E = \exp(-2\pi n\alpha/\omega) \qquad c = \cos(2\pi n\Omega/\omega)$$

$$s = \sin(2\pi n\Omega/\omega) \qquad c_k = \cos(\omega t_k) \qquad s_k = \sin(\omega t_k)$$

(their expression gives the coefficient of x_0 as $+1$; this does not affect their subsequent arguments for the impact oscillator as they set $x_0 = 0$). The eigenvalues of (5) are given by

$$\lambda_1, \lambda_2 = \tfrac{1}{2}[T \pm (T^2 - 4D)^{1/2}] \tag{8}$$

and the motion is stable if both eigenvalues lie within the unit disc on the complex plane (Iooss 1979).

4. One-impact orbits and their stability

For a one-impact period-n orbit t_k, y_k are given, after some algebra, by

$$t_k = \omega^{-1}\{\tan^{-1}(Y/Z) + \cos^{-1}(-X/W)\} \tag{9}$$

where

$$W^2 = Y^2 + Z^2$$

$$Y = \gamma(\omega\Gamma_+ + \psi\omega) + \delta(\psi\Gamma_-/\Lambda - \Lambda)$$

$$Z = \gamma(\omega\Gamma_-/\Lambda - \Lambda) - \delta(\omega\Gamma_+ + \psi\omega)$$

$$X = x_0(\Lambda - \omega\Gamma_-/\Lambda)$$

and

$$\Lambda = Es/\Omega \qquad \Gamma_\pm = 1 - Ec \pm \alpha\Lambda \qquad \psi = 2 - \Gamma_+$$

$$y_k = \omega[(\Gamma_+\Gamma_- + \Lambda^2)/(\psi\Gamma_- - \Lambda^2)](\delta c_k - s_k). \tag{10}$$

(All the above is worked through in greater detail by SH.) As $\omega \to 2n\Omega$, the denominator in (10) becomes small relative to the numerator; hence the resonance structure observed at $x_0 = 0$ by SH and TG, in which the maximum displacement from x_0 becomes large, also appears. At low β, where the asymmetry is more important these peaks are displaced towards higher ω. Bifurcations only occur when $\lambda = \pm 1$, for since $D = \lambda_1\lambda_2 < 1$, if the eigenvalues λ are complex then they are conjugate and $|\lambda| < 1$; therefore the only way an eigenvalue can pass through the unit circle is along the real axis, so no Hopf bifurcation is possible and at the bifurcation point $\lambda = +1$ (tangent bifurcation) or $\lambda = -1$ (flip bifurcation). So, rearranging (8)

$$D \mp T + 1 = 0. \tag{11}$$

Substituting from (6) and (7)

$$\Omega S_\pm y_k + 2\beta E c_k s \pm 2E x_0 s = 0 \tag{12}$$

where

$$S_\pm = 1 + E^2 \pm 2Ec.$$

A minimum condition for a one-impact orbit may be obtained for β from (9),

$$-X/W = \cos(\omega t_k - \phi)$$

where

$$\phi = \tan^{-1}(Y/Z),$$

W is linear in β, so writing $W' = W/\beta$,

$$\beta_{\min} = |X/W'|. \tag{13}$$

Below this value of β, a one-impact orbit of the given periodicity n does not exist. We may rearrange (12) to give the curves in the $\beta\omega$ plane on which bifurcation occurs.

Writing

$$G = \omega[(\Gamma_- \Gamma_+ + \Lambda^2)/\psi\Gamma_- - \Lambda^2] \qquad \delta' = \delta/\beta \qquad \gamma' = \gamma/\beta$$

so that

$$y_k = \beta G(\delta' c_k - \gamma' s_k),$$

the condition for $\lambda = \pm 1$ becomes

$$\beta_\pm [s_k M_\pm + c_k N_\pm] = \mp 2Ex_0 s \tag{14}$$

where

$$M_\pm = -\Omega S_\pm G\gamma' \qquad N_\mp = \mp 2Es + \Omega S_\pm G\delta'.$$

Now

$$c_k = -X\cos\phi/W - \sin\phi\,\sin[\cos^{-1}(-X/W)]$$
$$s_k = -X\sin\phi/W + \cos\phi\,\sin[\cos^{-1}(-X/W)]$$

therefore

$$c_k = -XZ/W^2 - [\pm Y(1 - X^2/W^2)^{1/2}/W]$$
$$s_k = -XY/W^2 + [\pm Z(1 - X^2/W^2)^{1/2}/W]. \tag{15}$$

The choice of sign in (15) is a problem, resulting from the choices of range of the inverse functions in (9), but the correct procedure seems to be to choose the sign so that it is the same as that of K (see below). This sign does not affect K because squares are taken, but it does affect y and hence which parts of the curves are eliminated. With some more algebra an expression for $\beta(\omega, \alpha, x_0, n)$ at the bifurcations is found:

$$\beta_\pm = (K_\pm^2 + X^2/W'^2)^{1/2}$$
$$K_\pm = \{X(M_\pm Y' + N_\pm Z')/W' \pm 2W'Ex_0 S\}/(M_\pm Z' - N_\pm Y') \tag{16}$$
$$Y' = Y/\beta \qquad Z' = Z/\beta.$$

Solutions with $y_k < 0$ are eliminated as they belong to orbits in $x > x_0$. Orbits which cross $x = x_0$ more than once must also be eliminated by checking through the path. If one of these orbits appears as some parameter is varied then there will be a discontinuity in the map.

In figure 2(b) this result is shown by the small stippled regions. If the parameters (β, ω) move into this region the one-impact orbit will disappear before the expected tangent bifurcation occurs; this is not a bifurcation and is responsible for the discrepancy between the theoretical and computed values of β at the disappearance of the one-impact orbit ($\omega = 1.5$) shown in table 1.

With yet more algebra K_+ is found to be identically zero, so that the condition (13) is implied by the condition $\lambda = +1$ (namely tangent bifurcation). The minimum of β may also be derived by considerations of the energy balance between impacts when the orbit is decomposed as a Fourier series. If $x_0 = 0$ then no tangent bifurcations can occur and the regions of stability become vertical strips centred on $\omega = 2n\Omega$, as found by SH for the slightly different system with a restitution coefficient.

The regions of stability for one-impact orbits for periods 1, 2, and 3 are shown by the large hatched regions in figure 2(a) (where $x_0 = +1$) and in 2(b) (where $x_0 = -1$).

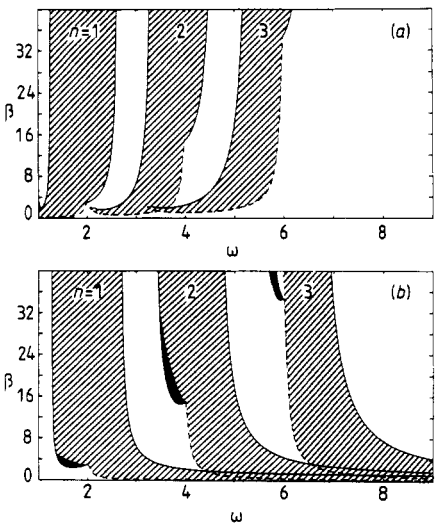

Figure 2. The regions of stability (shaded) for one-impact period-n orbits, with $n = 1, 2, 3$, $\alpha = 0.05$, (a) $x_0 = +1$ and (b) $x_0 = -1$. As $\beta \to \infty$, they become strips centred on $\omega = 2n\Omega$. Broken curves correspond to one eigenvalue passing through $+1$ and full curves to passing through -1. Stippled regions are inaccessible as the orbit penetrates beyond $x = x_0$ between impacts (see table 1).

Therefore, figure 2(a) refers to the case where the rest point of the impacting system is that of the unperturbed system, and figure 2(b) refers to the case where the wall displaces the oscillator under conditions of zero drive. Clearly for small frequencies and drive amplitudes the motion is stable in each case. The full curves refer to flip bifurcations ($\lambda = -1$) and the broken curves to tangent bifurcations. For the value of the damping coefficient of 0.05, the natural frequency Ω of the oscillator is 0.9975. Moving along one of the flip bifurcation boundaries (full curve) towards $\omega = 2n\Omega$ or approximately, $\omega = 2n$, s tends to zero and so the impact velocity tends to zero (as can be seen by rearranging (12) to put y_k on the left-hand side) and the oscillator does not reach the wall. There is a discontinuity in T at $\omega = 2n\Omega$ where the full curves reach the same point on each diagram in frequency-drive amplitude space. The impact velocity changes sign and so the motion occurs in the other half space, which leads to the line appearing on the other half of the figure. The same thing happens for the tangent bifurcations ($\lambda = +1$)—broken lines—and the broken and full curves are tangent at $\omega = 2n\Omega$ (not apparent on the scale of the figure) so the boundary of the stable regions is continuous and has a continuous first derivative. This can be seen by examining the equations of the curves (16), which are both continuous at $\omega = 2n\Omega$. K_+ vanishes identically and $K_-(\omega = 2n\Omega) = 0$. Therefore $\beta_- = \beta_+ = X/W'$ at $\omega = 2n\Omega$. The slope of β_- is

$$\frac{\partial \beta_-}{\partial \omega} = \frac{K_-(\partial K_-/\partial \omega) + \frac{1}{2}(\partial/\partial \omega)(X^2/W'^2)}{(K_-^2 + X^2/W'^2)^{1/2}}$$

and so at $\omega = 2n\Omega$ where $K_- = 0$ we find

$$\frac{\partial \beta_-}{\partial \omega} = \frac{\partial}{\partial \omega}\left(\frac{X}{W'}\right) = \frac{\partial \beta_+}{\partial \omega}.$$

Thus β_+ and β_- are tangent at $\omega = 2n\Omega$. This does not, of course, prove that β_+ and β_- have no other intersections, but we have examined plots for small intervals around $\omega = 2n\Omega$ for various n and have not found any sign that β_+ and β_- touch more than once.

As the damping coefficient α tends to unity the bands of stability become wider and for $x_0 = +1$, bifurcations with frequency constant and amplitude increasing disappear. In some places, e.g. at higher ω with $x_0 = -1$, the bands overlap and tangent bifurcations to another 1-impact orbit with periodicity one fewer become possible as the forcing amplitude is *decreased.* This overlap leads one to expect hysteresis, and an example is shown in figure 3. Only the first three zones are plotted.

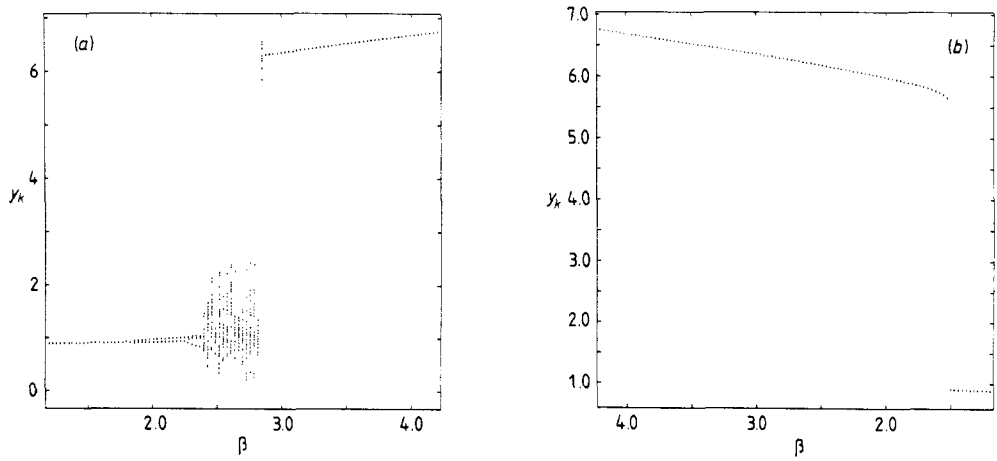

Figure 3. Hysteresis in transitions between single-impact orbits, (*a*) with increasing β and (*b*) with decreasing β, showing a $\lambda = +1$ bifurcation, calculated to be at $\beta = 1.495$. The upper line has period 2, the lower has period 1 ($\omega = 4.5$, $\alpha = 0.05$, $x_0 = -1$).

5. Brief program description

The programs used to produce the bifurcation diagrams with changes in β or ω both have essentially the same structure. The control parameter (β or ω) is altered in small steps. At each value of this parameter the system is allowed to evolve for a number of impacts, usually 100. Then for the next 100 or so impacts both the time between impacts $\Delta t_k = t_k - t_{k-1}$ and the velocity $y_k = \dot{x}_k$ are recorded and plotted on the diagrams as a function of the control parameter, which is then altered again.

Since the solution (x, y) is analytic between impacts, numerical integration is not necessary. The trajectory can be checked until it crosses $x = x_0$ and the root t_k can be found using a Newton–Raphson (NR) method. However, the calculation of the transcendental functions appearing in the exact solutions is costly in computer time, and since only the system variables at impact were of interest an approximate (and much faster) numerical integration was performed between impacts in order to give a seed for the NR root-finding routine. This then used the analytic solution to find the crossing time. The routine terminated when $|x - x_0| < \varepsilon$ where ε was typically of the order 10^{-5}.

This will not, of course give exactly the same phase space trajectories as a program computing analytic expressions, because each NR iteration will produce slightly different values of x such that $|x - x_0| < \varepsilon$. However, the trajectories for *periodic* solutions produced by the different methods will approach to within order ε. This, rather than rounding errors, will set the accuracy, although the convergence to periodic points ($\boldsymbol{p}_k$) on the Poincaré section is not limited by ε since on this scale the numerical map is more complicated, due to the structure imposed by the NR routine. The mapping which the computer performs (as distinct from the mapping which it simulates) comprises two sections, the first taking $\boldsymbol{p}_k$ to a point with $x > x_0$, and then a sequence of mappings produced by the NR iteration, which is contracting in the absence of nearby turning points. In chaotic regions, however, the trajectory may be seriously affected, for orbits which differed by less than ε at some time will diverge exponentially with time. (TG looked at a region of chaos between $\omega = 8$ and $\omega = 10$ and found a noisy exponential divergence.) Furthermore, for values of the parameters where more than one orbit is stable, transitions may occur either as a result of the inaccuracy or in the approach to equilibrium from the previous stable point. Of course, we can never be sure with numerical methods that a particular orbit is stable or not; here the orbits labelled 'stable' persisted for order 10^3 iterations. However, unstable subharmonics with lifetimes of order 10 s at 1.5 KHz have been observed using Robinson's apparatus, so it is not clear that all stable orbits deserve their name.

6. Results of the digital simulation

Table 1 summarises a few theoretical and experimental values of the control parameter β at the disappearance of stable one-impact orbits. Thus it would appear from the simulation that these are supercritical bifurcations. Passing through $\lambda = -1$ leads to stable 2-impact orbits of doubled period. If β is decreasing through $\lambda = +1$ with $x_0 = +1$ the orbit collapses, ceases to impact and returns to the linear steady state case. If $x_0 = -1$ the orbit cannot collapse and may fall into another stable periodic orbit with a lower threshold, or may drop into a region of chaos.

Figures 4(*a*), 4(*b*), 5, 6, 7 show some bifurcation diagrams with y_k recorded on the y-axis. Figures 4(*a*) and 5 show period doubling leading to chaos followed by the emergence of a three-impact period $n+1$ orbit; figure 6 shows a particularly complicated

Table 1.

			Thresholds					
			Upper			Lower		
x_0	ω	n	β_{theory}	β_{computed}	λ	β_{theory}	β_{computed}	λ
−1	3.0	1	6.423 828	6.423 ± 0.001	−1	0.188 899	0.189 ± 0.001	+1
−1	3.5	1	3.001 72	3.002 ± 0.001	−1	0.135 151		+1
−1	1.5	1				2.815 66	3.28±0.01	†
+1	3.0	2	6.818 58	6.819 ± 0.001	−1	0.780 939	0.781 ± 0.001	+1
+1	2.5	2	1.948 05	1.949 ± 0.001	−1	0.659 476	0.660 ± 0.001	+1

† Here there is a discontinuity in the map—the orbit touches $x = \dot{x}_0$ between t_k and t_{k+1}. $\alpha = 0.05$.

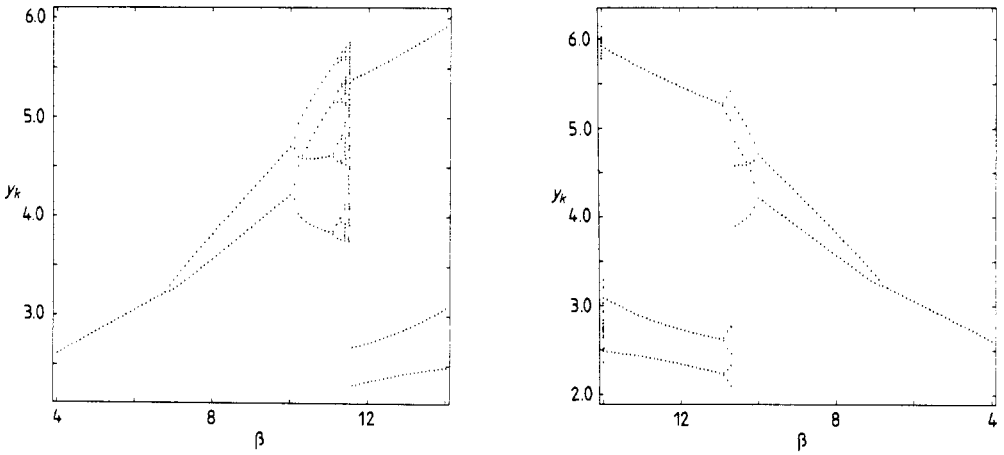

Figure 4. (*a*) Period doubling from 1-impact period-2 orbit and emergence of stable 3-impact orbit. (*b*) The same, with decreasing β, showing coexistence of 3-impact orbit with stable 2-impact orbits near $\beta = 11$ ($\omega = 3.0$, $\alpha = 0.05$, $x_0 = +1$).

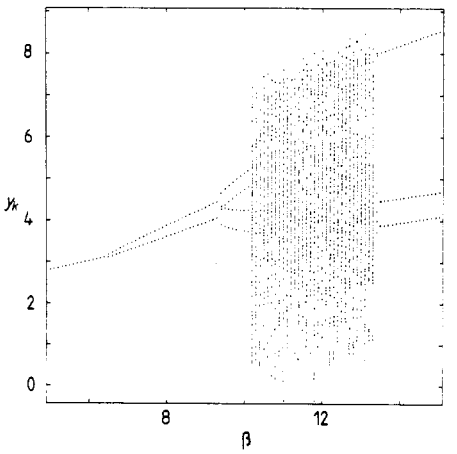

Figure 5. The same as in figure 3 but with $x_0 = -1$. The structure is similar but the 3-impact orbit is not coexistent with stable 2-orbits.

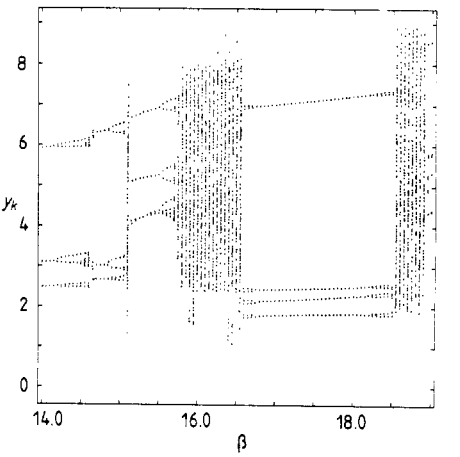

Figure 6. As figure 3 but at higher $\omega(14)$, showing many transitions between stable periodic orbits.

set of stable orbits separated by transitions and chaos, while figure 7 shows two- and four-impact orbits not resulting from period doubling. The four-impact orbit occurs in a region where a one-impact period-two orbit is also stable.

We have already seen that there can be more than one stable periodic orbit for some sets of parameters. Periodic and chaotic orbits may also coexist for certain regions in (β, ω, α) space. If there are transitions between them on altering a parameter hysteresis typically occurs. Whenever or not the transition points on the diagrams are actually where the first orbit ceases to be stable is open to question. The attracting sets in the Poincaré section for coexistent orbits may be close, so that after a small increase in the control parameter the last point for the previous value of β or ω, can lie in the attracting set of another orbit. This would result in a transition whose position varies with the size of the increment of the control parameter. It is this effect that is

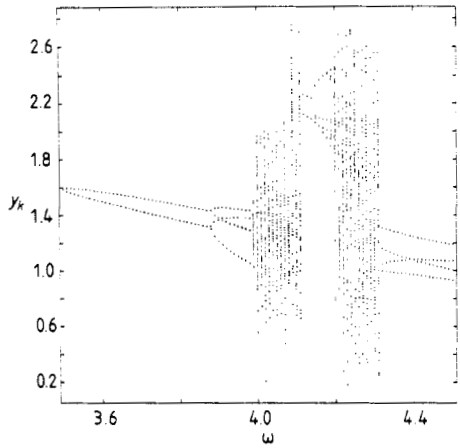

Figure 7. 2-impact period-3 and 4-impact period-4 orbits not resulting from period doubling. The 2-impact orbit nearly always appears between 1-impact regions.

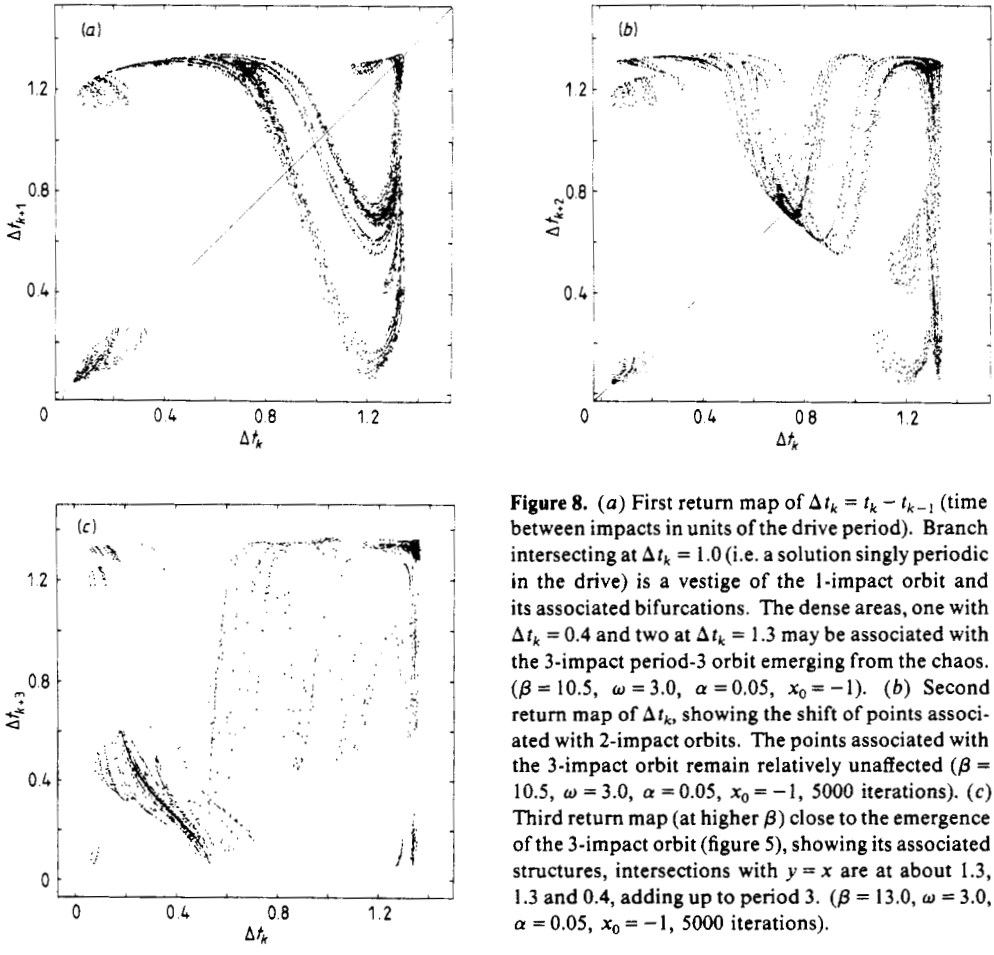

Figure 8. (*a*) First return map of $\Delta t_k = t_k - t_{k-1}$ (time between impacts in units of the drive period). Branch intersecting at $\Delta t_k = 1.0$ (i.e. a solution singly periodic in the drive) is a vestige of the 1-impact orbit and its associated bifurcations. The dense areas, one with $\Delta t_k = 0.4$ and two at $\Delta t_k = 1.3$ may be associated with the 3-impact period-3 orbit emerging from the chaos. ($\beta = 10.5$, $\omega = 3.0$, $\alpha = 0.05$, $x_0 = -1$). (*b*) Second return map of Δt_k, showing the shift of points associated with 2-impact orbits. The points associated with the 3-impact orbit remain relatively unaffected ($\beta = 10.5$, $\omega = 3.0$, $\alpha = 0.05$, $x_0 = -1$, 5000 iterations). (*c*) Third return map (at higher β) close to the emergence of the 3-impact orbit (figure 5), showing its associated structures, intersections with $y = x$ are at about 1.3, 1.3 and 0.4, adding up to period 3. ($\beta = 13.0$, $\omega = 3.0$, $\alpha = 0.05$, $x_0 = -1$, 5000 iterations).

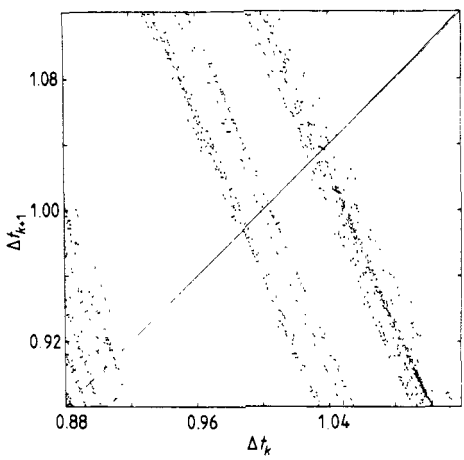

Figure 9. An expanded view of figure 8(*a*) with 70 000 iterations, showing the Cantor set-like structure.

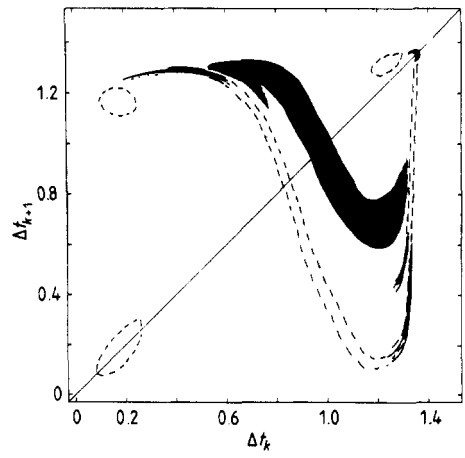

Figure 10. Schematic diagram of figure 8(*a*), showing structures in return map associated with the different orbits emerging from chaos.

thought to be responsible for the failure to each the accumulation point in figure 5. With smaller increments the higher n 2-impact orbits appear, and the accumulation point is $10.292 < \beta_{acc} < 10.293$. This is distinct from the type of transition where the orbit touches $x = x_0$ between t_{k-1} and t_k.

The return maps of Δt_k and y_k (figures 8(*a*), 8(*b*), 8(*c*), 9, 10) show a high degree of folding, and their transverse structure is Cantor set-like, (figure 9 is a blow-up of a region in figure 8(*a*) with 70,000 iteractions) strongly suggesting that the attractors have fractional dimension.

The full return map is a surface embedded in the four-dimensional manifold $(t_{k-1}, t_k, y_{k-1}, y_k)$. We have taken two submanifolds (t_{k-1}, t_k) and (y_{k-1}, y_k), and the sections of the attractor of the return map so revealed seem to have dimension between one and two, suggesting that the full map has attractors with dimension between two and three. (Using t_k instead of the phase at impact, $t_k \bmod 2\pi/\omega$, does remove some information from the map, since (t_k, y_k) do not uniquely determine (t_{k-1}, y_{k-1}); the phase is required. However, when t_k is expressed in multiples of the driving period, the remnants of periodic orbits are easy to see on the return maps.) The intersections of the curves with the line of unit slope occur very close to the values expected from the periodic orbits close by. The first, second and third (at higher β) return maps in the chaotic region just after the accumulation point in figure 5 show two distinguishable structures, depicted schematically in figure 10, associable with the two different orbits (periods two and three) that emerge from the chaos.

The large shaded region in figure 10 shows the parts of figure 8 that are associated with the cascade of period doubling bifurcations preceeding the chaos (which occurs for $10 < \beta < 13.5$ in figure 5(*a*)) whereas the three sets of full lines at (1.3, 0.4), (1.3, 1.3), (0.4, 1.3) depict those parts which can be identified with the period 3 motion that appears above $\beta = 13.5$ in figure 5(*a*).

The inner structure shows branches which intersect $t_{k+1} = t_k$ with negative slope of magnitude greater than one. At lower β, one of these will give the 1-impact period-1 stable orbit. The second return map shows this structure shifted, with two intersections corresponding to the 2-impact orbit existing when $6.4 < \beta < 9.5$, while the other structure

is little affected. The third return map shows that this structure corresponds to a 3-impact orbit which, as β is increased becomes more prominent (figure 8(a)), i.e. the system spends more time in the unstable 3-impact region.

One would expect if the system lingers in unstable orbits (here a 3-impact orbit) that peaks should be apparent in the frequency spectrum of $x(t)$, and indeed such peaks are observed (Usher and Jefferies) in the system of coupled impact oscillators at subharmonic frequencies of the drive. Figure 11 shows the first return map of y_k, the impact velocity. The structure of this map take longer (more iterations) to emerge, but the complicated folding is here very apparent. Again, there are 'preferred' regions around the sites of formerly stable periodic attractors.

The Poincaré sections ($\omega t_k \bmod 2\pi, y_k$) (figures 12($a$), 12($b$)) also show separation into regions belonging to different orbits, each region showing an attractive Henon-like

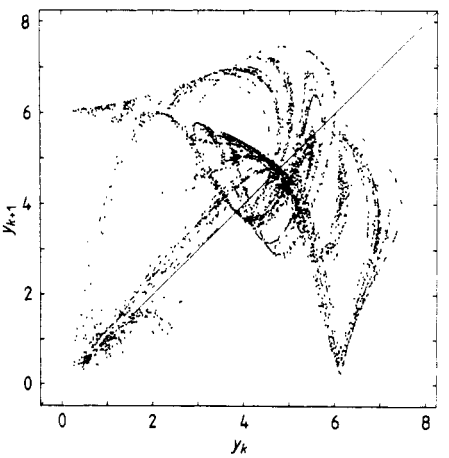

Figure 11. The first return map of the impact velocity y_k for the same parameters as figure 8(a).

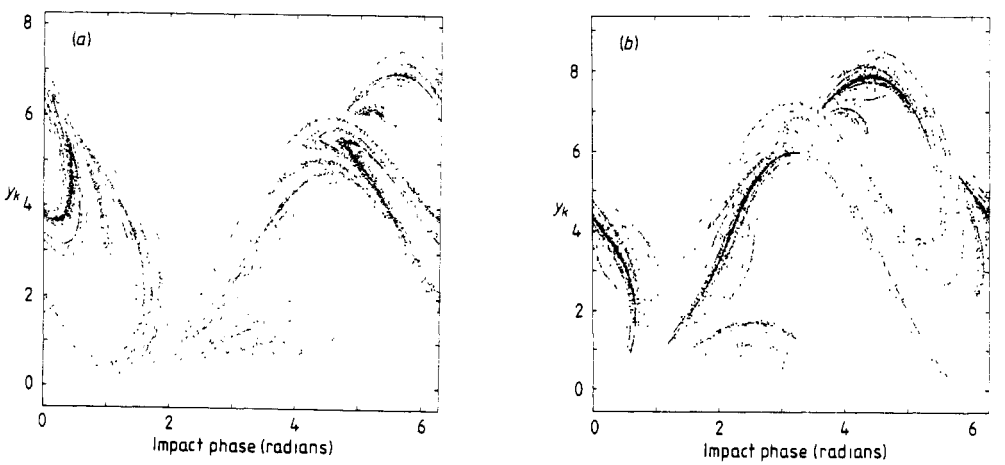

Figure 12. (a) Poincaré section taken at $x = x_0$, $y > 0$, just after period doubling from 1-impact orbit, ($\beta = 10.5$, $\omega = 3.0$, $\alpha = 0.05$, $x_0 = -1$, 5000 iteractions) (b) and at higher β showing predominance of 3-impact structure and phase shift.

structure. In figure 12(*b*), closer to the emergence of the 3-impact orbit, there are bare patches not found in figure 12(*a*), presumably belonging to the aftermath of the cascade of bifurcations from the single impact orbit.

The collision of these two attracting basins is conjectured to provide an explanation for the crisis (Grebogi *et al* 1982) of the attractor in figure 5, where the bounds of the motion undergo a discontinuous change. Jeffries and Perez (1983) have also observed this kind of crisis, which is distinct from that caused by the interaction of an unstable and a chaotic attractor, as outlined by Grebogi *et al* (1982).

7. Conclusions

Impact oscillators of this sort may be considered as an idealisation of simple vibrating impacting systems, such as moored ships and beams constrained by stops. Although the first derivative is discontinuous, and hence non-physical, it is relatively easy to obtain computational results since the motion between impacts is simple and the time-expensive computation can be restricted to the region of phase space near impact. Analytic results for the case of stable orbits with one kind of impact repeated after an integer number of periods agree well with the computer simulation. The simplicity of the system belies the structure found in its motions.

The return maps cannot be expressed in analytic form and in the chaotic region display folding and show attractors with probable fractional dimension, but their local structure reflects the behaviour of nearby stable orbits. The mapping has many discontinuities, especially for $x_0 = +1$, which provide much of the interest. One way to make the mapping more tractable is to drive the system impulsively. This would allow orbits that previously would have crossed $x = x_0$, but the same single impact period n orbits should appear, with their associated bifurcations. This system is less interesting physically but more tractable to analysis.

References

Cascais J, Dilao R, and Noronha da Costa A 1983 *Phys. Lett.* **93A** 213
Grebogi C, Ott E and Yorke J A 1982 *Phys. Rev. Lett.* **48** 1507
Henon C 1976 *Commun. Math. Phys.* **50** 69
Iooss G 1979 *Bifurcation of maps and applications* (Amsterdam: North-Holland)
Jeffries C and Perez J 1982 *Phys. Rev.* **26A** 2117
—— 1983 *Phys. Rev.* **27A** 601
Manneville P and Pomeau Y 1979 *Phys. Lett.* **75A** 1
Ott E 1981 *Rev. Mod. Phys.* **53** 655
Perez J and Jeffries C 1982 *Phys. Rev.* **26B** 3460
Pomeau Y and Manneville P 1980 *Commun. Math. Phys.* **74** 189
Robinson F N H 1982 *Preprint, Clarendon Laboratory, Oxford*
Shaw S W and Holmes P J 1982 *Preprint, Cornell University*
Thompson J M T and Ghaffari R 1982 *Phys. Lett.* **91A** 5
Usher A and Jefferies D J 1983 *Phys. Lett.* **98A** 396